

NUMERICAL MODELLING OF THE UNSTEADY INTERACTION BETWEEN PROBE AND FLOW IN AXIAL TURBOMACHINERY

J. Seume¹, F. Herbst¹

¹Laboratory of Turbomachinery and Fluid
Dynamics
University of Hannover

D. Missirlis², K. Yakinthos², A. Goulas²

²Laboratory of Fluid Mechanics and
Turbomachinery
Aristotle University of Thessaloniki

ABSTRACT

The present work investigates the unsteady interactions between a four-hole pneumatic probe, the flow and the blades of the 4AV axial compressor of the Turbomachinery Laboratory of the Leibniz University of Hannover (TFD). The investigation was necessary in order to comprehend the exact mechanisms that can affect the accuracy of experimental measurements when the latter are carried out inside a turbomachine. The analysis was performed numerically in the Laboratory of Fluid Mechanics and Turbomachinery of Aristotle University of Thessaloniki with the use of the commercial flow solver Numeca FINE and already available experimental data were used for the validation of the computations.

INTRODUCTION

One of the main interests of engineering has always been the optimization of industrial processes. This trend is, also, maintained in the field of turbomachinery. In order to improve the overall performance in a turbomachine, reliable data describing the flow field inside the machine are needed. Based on these data, modifications can be suggested so as to improve possible problematic regions and increase the efficiency. These modifications can be performed completely experimentally or with the use of numerical methods. However, since CFD is not always capable of predicting completely accurately all physical phenomena of the flow, the validation with experimental data is necessary. In order to obtain these data pneumatic probes are widely used for measuring pressure, velocity, flow angle and, when supplied with a thermoelement, temperature. Unfortunately, the use of pneumatic probes does not always cover the need for reliable data and, more specifically, at high velocity flows their field of application inside the close axial gaps of turbomachines is limited by the unsteady interactions between the probe, the flow and the blades of the turbomachine. These interactions can be so important that they can affect and falsify the experimental results causing significant decrease in the quality of the measurements and limit the acceptable range of use of pneumatic probes. Thus, the quality of experimental data depends heavily on these interactions and an investigation is necessary

in order to verify and correct them. Such an effort is made in the present work where the commercial flow solver Numeca FINE is used to investigate, numerically, the interactions between probe, flow and blades of the 4AV axial compressor, Fig.1, and a four-hole pneumatic probe, Fig.2.

The 4AV axial compressor

The four stage high-speed axial compressor 4AV is a research compressor. Experiments were carried out in the axial gap behind the blade rows and at 4 positions inside the first stator row at the rotational speed of 17100 rpm. The compressor generates an overall total pressure ratio of 2.7. The mass flow was metered by an orifice. The axial inlet flow conditions were measured with a Prandtl tube and a temperature probe. Measurements for the outlet flow conditions and the flow field between the blade rows were carried out by a pneumatic four-hole probe including a temperature sensor. Efficiency and overall total pressure ratio were measured by two rakes in the outlet.

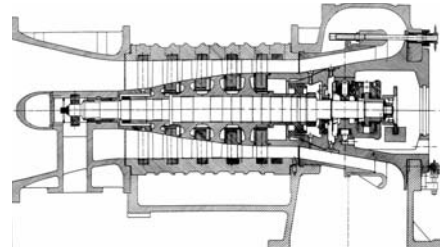


Fig.1. The 4AV axial compressor

The four-hole cobra probe

The probe used for this simulation and for the experimental measurements is a steady measuring four-hole pneumatic probe named "Sonde F", Fig.2. Developed during a former "FVV" research project it was designed for the duct region close to the hub, which is indicated by the position of the γ -angle hole (4) above the total-pressure hole (1). The probe consists of four small tubes, two central and two placed in a symmetrical arrangement. Each of these tubes is providing pressure values to a digital manometer. The head of the cobra probe, the flow angles, the velocity vector, \vec{C} , and its three components are presented in Fig. 3. Since the flow around the probe depends on the conditions of the upstream flow and on the flow angles α and γ , the measured

pressures in the pressure holes are not equal to the ones of the undisturbed flow field. To acquire the actual value of the pressures inside the flow field, proper calibration coefficients have to be defined which describe the relation between the measured values and the real quantities of the upstream flow. After the calibration, the probe is capable of measuring, simultaneously, total and static pressure, velocity magnitude and flow angle. At the same time, total temperature measurements can be carried out since the probe is supplied with a thermoelement. The general idea of the calibration lies in the experimental derivation of some characteristic, Mach dependent, calibration coefficients correlating the actual flow quantities with the measurements of the pressure holes for known flow conditions. Details can be found in Braun and Riess [2]. At the next stage, during the experimental measurements, when the probe is inserted in an unknown flow field the inverse procedure is followed to compute the actual flow quantities since the pressure coefficients can be calculated by the measurements of the pressure holes.

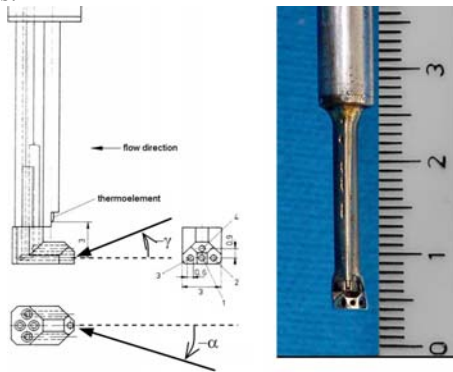


Fig.2. Four-hole cobra probe (Probe F)

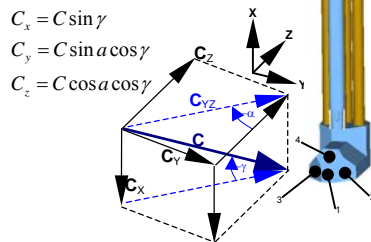


Fig.3. Definition of flow angles and velocity components

Due to its position on the probe geometry, the measurements of the pressure hole 1 can be linked to the total pressure, while the ones of the pressure holes 2 and 3 can be correlated to the static pressure as:

$$p'_{total} = p_1$$

$$p'_{static} = \frac{(p_2 + p_3)}{2}$$

The yaw angle α can be measured by the balancing method, since it is usually easy to rotate the probe around its shaft axis until the pressure holes 2 and 3 measure the same pressure value. The pressures p_2 and p_3 can easily be measured with a

manometer and α can be read off directly. However, the pitch angle γ cannot be determined by the balancing method, as it is not applicable to rotate the probe in a turbomachine. For this reason the so called pressure differential method is more common. Therefore, the installation of the probe is done under a convenient angle, mostly rectangular to the axis of the duct. Since the flow encounters the probe in a specific angle the measured values for the similar to the total pressure p'_{total} as well as for the similar to the static pressure p'_{static} are not equal to the ones of the undisturbed flow. The determination of the calibration coefficients is done by referring them to the similar to the dynamic pressure $q' = p'_{total} - p'_{static}$ which is measured by the probe. Thus, the following non-dimensional coefficients are defined:

1. For α the YAC (Yaw-Angle-Coefficient):

$$YAC = \frac{\Delta p'_{\alpha}}{q'} = \frac{\Delta p'_{\alpha}}{p'_{total} - p'_{static}} = \frac{p_2 - p_3}{p_1 - \frac{(p_2 + p_3)}{2}}$$

2. For γ the PAC (Pitch-Angle-Coefficient):

$$PAC = \frac{\Delta p'_{\gamma}}{q'} = \frac{\Delta p'_{\gamma}}{p'_{total} - p'_{static}} = \frac{p_1 - p_4}{p_1 - \frac{(p_2 + p_3)}{2}}$$

3. For total pressure the TPC (Total-Pressure-Coefficient):

$$TPC = \frac{P_{tot,Pr} - p'_{total}}{q'} = \frac{P_{tot,Pr} - p'_{total}}{p'_{total} - p'_{static}} = \frac{P_{tot,Pr} - p_1}{p_1 - \frac{(p_2 + p_3)}{2}}$$

4. For static pressure the SPC (Static-Pressure-Coefficient):

$$SPC = \frac{P_{stat,Pr} - p'_{static}}{q'} = \frac{P_{stat,Pr} - p'_{static}}{p'_{total} - p'_{static}} = \frac{P_{stat,Pr} - p_3}{p_1 - \frac{(p_2 + p_3)}{2}}$$

The index Pr indicates quantities measured by Prandtl's tube. Hence, the pressures of the flow field can be computed as:

$p_{total} = p'_{total} + TPC \cdot q'$ and $p_{static} = p'_{static} + SPC \cdot q'$
Since the coefficients depend on the Mach number and the Mach number itself depends on the static and total pressure, it is obvious that an iteration process is inevitable. The calibration data are calculated according to measurements in a high-velocity wind tunnel (Appendix A). Finally, the equations of the compressible flow ($Ma > 0.3$) are used to calculate the velocity magnitude:

$$T_{total} = T_{static} + \frac{C^2}{2c_p}$$

$$T_{static} = T_{total} \cdot \left(\frac{p_{static}}{p_{total}} \right)^{\frac{\kappa-1}{\kappa}}$$

$$C = \sqrt{2(T_{total} - T_{static})c_p}$$

CFD and turbulence modeling

The turbulence models used in this work are the Baldwin-Lomax [1,7] and the Spalart-Allmaras [8]. Compared to two-equation models like the $k - \epsilon$ model, they require lower computational expense and offer a higher

numerical stability. Furthermore, Baldwin-Lomax and Spalart-Allmaras are recommended for flows with a strong pressure gradient like the one of the compressor at hand [5]. So, in case of this work with its hardly foreseeable numerical behaviour and due to the limitation in the computational performance, both models seem to be appropriate. Due to its robustness and faster performance the Baldwin-Lomax model is applied on the first computations concerning the grid dependence of the solutions of the compressor mesh and the overall behaviour of the probe mesh while the Spalart-Allmaras model is applied for the final computations, which are used for the evaluation of the probe measuring values.

The CFD flow solver NUMECA FINE 6.13 is used for the computations on a Dual CPU AMD Athlon MP 1800+ 1,53 GHz machine with 2 GB of RAM available. IGG 4.9-2 and AutoGrid 5.1 software are used for the creation of the computational grid while CFView 4.9-2, post processing software, is used for the evaluation of the results.

Simulating the flow field in the 4AV axial compressor without the probe

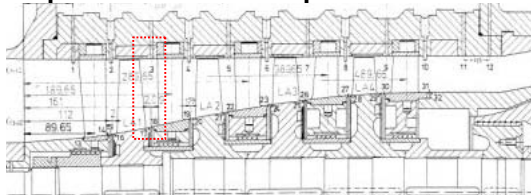


Fig. 4. Axial measurement positions of the 4AV compressor (red line indicates the probe position)

The investigation of the interaction between the pneumatic cobra probe and the first rotor of the 4AV axial compressor cannot be performed for the whole region of the compressor due to excessive memory and CPU requirements. Thus, in order to proceed and achieve an appropriate simulation of the flow field, only the IGV and the first stage (containing Rotor 1 and Stator 1) are modeled. However, since the IGV is composed of 26 blades, the Rotor 1 of 23 blades and the Stator 1 of 30 blades, the computations for a complete 360° model of the compressor would still remain impossible. Thus, a characteristic blade passage was selected as the computational domain, Fig.5.

The computational domain was composed of six blocks each of which was corresponding to a specific angle of the 360° geometry of the compressor depending on its periodicity. The boundary conditions which were used for the computations are presented in Fig.5. At the inlet of the computational domain total conditions of pressure and temperature were used while at the outlet the static pressure was imposed. At the side limits of the computational blocks a periodic

boundary condition was applied with the number of periodicity being set at such a value so as to simulate the effect of the IGV, the Rotor 1 and the Stator 1 blades for the 360° of the compressor. Between the different blocks and when the limits of the blocks match a connection (CON) boundary condition was applied so that the flow quantities can be computed as the flow travels from one computational block to the other. However, specifically for the limits of block 3, which contains Rotor 1, a different approach was followed.

The coupling and interaction between rotating (Rotor 1) and non-rotating blocks (IGV and Stator 1) is an aspect of main interest when simulating turbomachinery. Especially the relative motion between successive blade rows is a major source of unsteadiness that can affect the flow locally as well as globally if it travels through the next rows. Thus, the rotor-stator interface must exchange mass, momentum and energy fluxes. The model chosen in this work is the Default Mixing Plane Approach with conservative coupling by pitchwise rows as boundary condition. It is considered to be a steady method, even though it simulates rotated blocks, which averages all quantities at the interface pitchwisely [4, p5-15]. Therefore, the flow field from the inner cells is extrapolated onto the surface in a first step and then it is interpolated onto meshes that share the same spanwise grid point distribution on both sides of the interface. On this dummy cells the pitchwise averaged variable of one side is mixed with the variable of the other side depending on the chosen boundary condition. Finally, the result is interpolated back onto the initial mesh interface and the dummy cells are set to impose the calculated variables on the interface. This approach ensures a strict global conservation through the interface and was applied in this work as it is considered to be very robust numerically. This coupling takes place through the definition of a special boundary condition (ROT) in the interface before and after block 3 of the Rotor 1. At the same time block 3 was set to have a rotational speed of 17100 rpm, the same as Rotor 1 in the experiments.

As long as only the region of the first one and a half stages of the 4AV compressor (IGV, Rotor 1, Stator 1), was investigated, an outlet must be created after Stator 1 so as to ensure a sufficient flow development at outlet. For this reason, the outlet of the stator was prolonged by approximately 200 mm, in order to be able to impose a boundary condition at the outlet, which would not be affected by the flow field in the direct vicinity of the stator and which would be suitable to the physics of the problem. However, the hub line of the extension was not following the angle of the 4AV hub and it was designed as a parallel to the shroud. Thus, the streamed plain behind stator 1 remained even and

there was no acceleration or pressure recovery on the flow field.

The accuracy of the simulations of the computational results must be validated towards experimental values. Since the quality of the simulations depend on the computational grid a proper grid have to be found for which the results would be as grid independent and close to the experimental values as possible. Thus, several grids of different numbers of grid points were computed and compared for their quality. For these computations the Baldwin-Lomax model was used, as it is faster and requires less computational expense than Spalart-Allmaras model.

At the first step, the commercial software AutoGrid was used to create the entire compressor mesh (initially without the probe inside the compressor). Its automated creation process required the specification of a certain number of settings to generate an applicable grid. Most of the used settings in this work regarding point distribution, clustering, smoothing etc., originated from suggestions from previous simulations with AutoGrid [4-6].

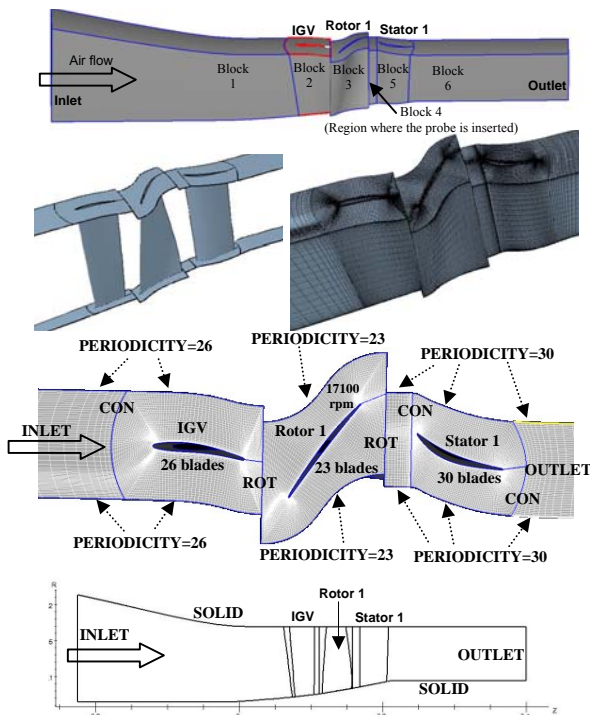


Fig.5. Computational domain, geometry, grid, boundary conditions and meridional view of the simulation

Because of the direct influence on the computational results, the number of grid points and their distribution among the three dimensions was of special interest. It was essential that the results were physically reasonable and, in the best case, approximated experimental results. If the grid was too coarse, it will not represent the flow field adequately and some effects would not be captured.

In the present work, six grids were investigated ranging from, approximately, 960000 to 2400000 computational points. Two operating points were investigated, which were chosen because they could be compared to experimental values. It was decided that the comparison between the computed mass flows and the measured ones at specific operating points (same boundary conditions with the experiment) would be the crucial factor so as to evaluate the mistake of the simulation and the quality of the created grids. After some preliminary computations two grids were selected as being the most proper for further computations. The first one was having 1.87 million grid points and a relative mass flow error of 2.8% towards the experiments and a coarser second one having 1.12 million grid points and a relative mass flow error of 3.2%. The remaining mass flow error can be attributed to the incomplete simulation of the compressor including only the first stage and the IGV.

As the interaction of the probe and the rotor was to be investigated when the 4AV compressor was working at its highest efficiency, design point 2b, the boundary conditions for this point have to be found by computing the characteristic curve of the compressor. The 1.12 and 1.87 million points grids were computed with varied static pressures at outlet while keeping the inlet conditions untouched (the increase of the static outlet pressure $p_{stat,out}$ led to a decrease of the mass flow for both grids) and the behaviour of the isentropic efficiency was examined. In order to gather useful results for the final computations with the probe, Spalart-Allmaras was used as the turbulence model. The results of the 1.12 (named as *less* in the diagrams) and 1.87 (named as *full* in the diagrams) million points grids were compared with experimental data set [3] in the characteristic curve of Figure 6. A comparison with the CFD results reveals significant differences in the absolute values. On the other hand the CFD results present a similar curve tendency.

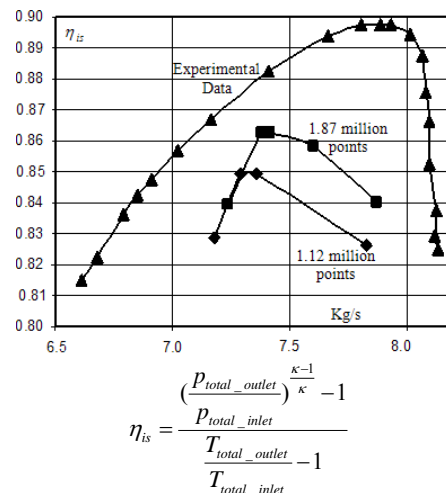


Fig.6. Characteristic curve
Thessaloniki, GREECE
21- 22 September 2006

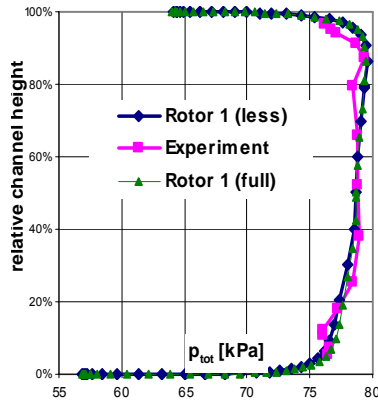


Fig. 7. Total pressure after rotor 1

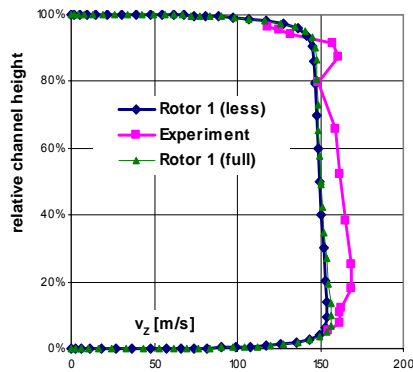


Fig. 8. Axial velocity profile after rotor 1

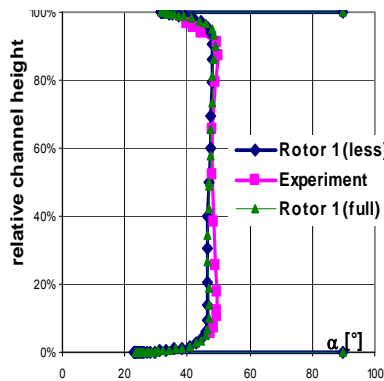


Fig. 9. Angle α after rotor 1

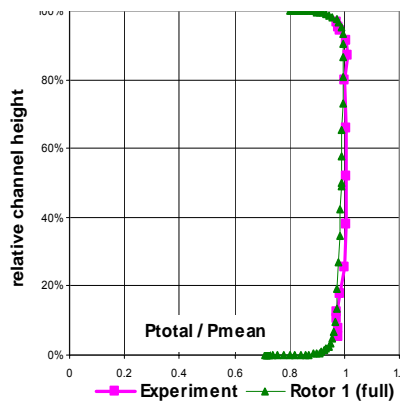


Fig. 10. Non-dimensional total pressure after rotor 1

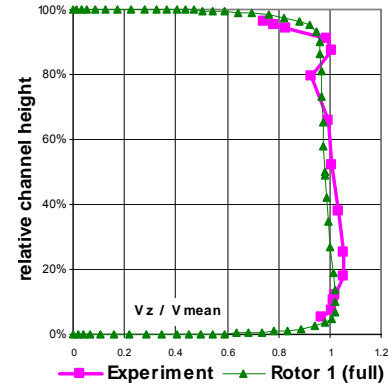


Fig. 11. Non-dimensional axial velocity after rotor 1

Case	m [kg/s]	π_{stat}	η_{is}
Operation point 2b_exp	7.821	1.262	0.898
Without probe 1.87 million (full)	7.4203	1.1713	0.8625
Without probe 1.12 million (less)	7.3561	1.1702	0.84951

$$\pi_{stat} = \frac{P_{static_outlet}}{P_{static_inlet}}$$

Table 1. General performance data of the empty grids and the experiment.

Additional results can be found in Fig. 7 to 9. As it can be seen the profiles are nearly identical for both grids. Only minor differences exist, which can be attributed to the coarser and not so detailed resolution of the 1.12 million grid. The general performance values, Table 1, show differences between the two grids in the efficiency and in the mass flow. However, the gap to the experiment is obvious for both grids. These discrepancies can be attributed to the incomplete simulation of all effects of the compressor.

Simulating the flow field in the 4AV axial compressor with the probe

After investigating the compressor mesh and creating two sufficient grids with 1.12 million and 1.87 million points, the next step was the insertion of the probe. Therefore, the rectangular block 4 after rotor 1 and before stator 1 was replaced by the mesh of the probe, Fig. 12. Since this grid was already created properly taking into account the geometrical conditions at this specific axial position, the insertion of the probe required no extra effort, apart from the creation of an adequate grid capturing into details the probe geometry.

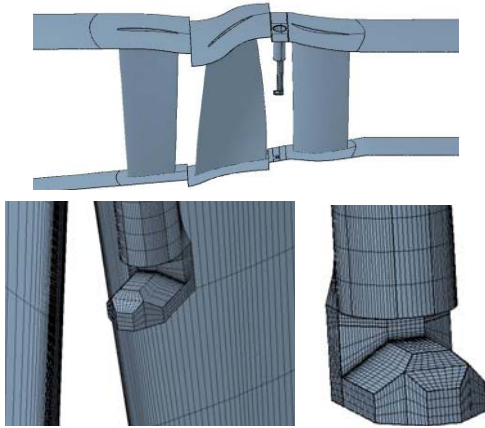


Fig.12. The 4AV axial compressor with the probe

Only the boundary conditions of the probe grid outer faces had to be set with some extra thoughts. The side faces of block 4 as well as of all the other blocks are set as periodic boundaries (PER), with a periodicity depending on the blade number of their stage as for the case without the probe.

With the usage of periodic boundary conditions in a turbomachinery simulation the flow solver assumes that the flow is periodic in pitchwise direction. Therefore, it only solves the flow field of one blade per stage. By multiplying the resulting quantities by the periodicity a solution for the 360° flow field is obtained. This whole procedure reduces the number of required meshed blades per stage to one, decreases the number of grid points and makes a grid of a whole compressor computable with the given computer hardware.

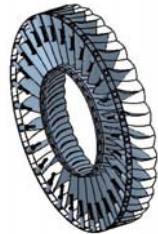


Fig.13. The "thirty probes problem"

Unfortunately, the assumption of a pitchwise periodic flow field and geometry neglects irregular phenomena or effects with a differing periodicity, for example a probe. If the probe mesh would be treated like the placeholder block 4 with the periodicity of the stator (30), it would actually lead to a solution of a flow field with thirty probes in pitchwise direction after rotor 1, Fig.13, causing a high blockage effect in the duct. Thus, a lower mass flow and efficiency would occur compared to the desired case of one probe after Rotor 1.

Consequently, in order to weaken the blockade of the duct, the probe mesh should be extended in the pitchwise direction. Instead of meshing all thirty stator blades a reasonable approach would be to mesh only three or five stator blades. This attempt would decrease the number of

probes to ten and six, respectively, and was applied to both compressor meshes (with 1.87 and 1.12 million points). The computer hardware limited the maximum number of grid points which is computable with Spalart-Allmaras (Baldwin-Lomax would allow more points). So the addition of two stator blades to the denser 1.87 million points grid marked the ceiling for this setup with about 3.6 million grid points. The finally computed meshes with probe between Rotor 1 and Stator 1 were the following:

- Dense grid with probe and one stator blade : 2 283 923 points (With_full)
- Dense grid with probe and three stator blades: 3 661 425 points (2pass_full)
- Coarse grid with probe and three stator blades: 2 356 925 points (2pass_less)
- Coarse grid with probe and five stator blades: 3 166 235 points (4pass_less)

In all cases one (2pass) or two (4pass) empty blocks, same as the original block 4, were added on both sides of the 12° probe grid. Figure 14 illustrates the configuration with three and five stator blades. The addition of blocks upstream was not necessary because the special rotating boundary condition (ROT) between the rotor block and the probe grid only required that the linked faces were in the same axial plane. The edges of these faces did not have to coincide.

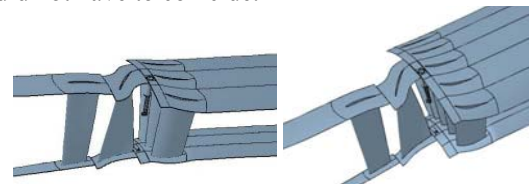


Fig.14. First 4AV stage with probe and three stator blades (2pass) and five stator blades (4pass)

The four grids were computed with the Spalart-Allmaras model at the operating point 2b. A first investigation of the computations of the denser grid (1.87 million points) revealed a mistake in the alignment of the probe regarding its yaw angle α and the calibration data. The probe with an allowed measuring range of $\alpha = \pm 15^\circ$ was inserted with $\alpha = 0^\circ$ (towards the axial velocity component at the inlet). However, the upstream flow had an angle of -43.4° , Fig.15, so that it was necessary to rotate the probe by -43° and the computation with three stator blades to be repeated (With_rot_2Pass).

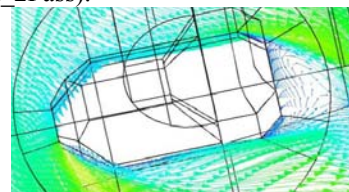


Fig.15. Flow field at the probe head

Table 2 presents the general performance data for all computations of the denser grid with

probe and without probe at the design point 2b. The first simulation with probe at $\alpha = 0^\circ$ and one stator blade (With_1) led to the expected decrease in all quantities due to the thirty probes which were blockading the duct. This effect was minor for the pressure ratio and significant for the isentropic efficiency. Furthermore, the calculation of the relative mass flow error revealed a difference of 10.55% to the empty case. By adding two stator blades (With_1_2pass) and weakening the blockade, all quantities increased and the error decreased. This improvement of the performance data justified the neglecting of the one stator case regarding the rotation of the probe and the repetition of the computation. So for the final calculation of the probe measurement values only the "With_rot_2Pass" case was of interest where the probe is rotated and two empty blocks are added.

The investigation of the coarser grid after the probe was rotated, Table 3, revealed the same tendency in the differences between the empty (Without_less) and the three stator case (With_less_2pass) as in the computations above. Furthermore, the values of the additional five-stator case (With_less_4pass) came even closer to the results of the empty grid. With a relative mass flow error of 1.92% and a difference of about 5% in the efficiency, this setup minimized the inaccuracy originating in the periodic boundary condition of the probe block regarding the general performance data.

Derivation of flow quantities – Comparison with experimental data

In order to calculate the magnitude of the velocity \vec{C} and the flow angles α and γ at the chosen measurement position via the probe and its calibration data, respectively, the pressures at the geometric positions of the measurement holes have to be determined. The present work uses two ways to obtain these four pressures:

1. Local values are taken at the middle point of the holes onto the probe surface.
2. Following the grid structure on the surface, areas are defined which approximates the holes as good as possible. Then the surface averages of the pressures are taken in these areas.

Figure 16 illustrates both ways for the "With_rot_2pass" case and shows that the pressures vary highly within the defined areas indicating that the surface averages are more representative for the actual pressure of the holes than the local values.

Table 4 reveals an overall higher pressure level of the denser grid (With_rot_2pass), whereas a comparison of the results of the coarser grids shows minor differences for most of the values. Only the local values of p_2 (of With_less_2pass and

With_less_4pass) show a significant difference of about 1200 Pa, which reduces to about 500 Pa for the surface averages of the same quantity. This change is the effect of the compensating effect of the surface-average function taking into account the distribution of the pressure within the defined area.

Case	stator blades	mass flow [kg/s]	relative mass flow error	π_{stat}	η_{is}
Without_full	1	7.4204	0.00%	1.1713	86.25%
With_1	1	6.6377	10.55%	1.1621	68.65%
With_1_2pass	3	7.1559	3.56%	1.1678	78.46%
With_rot_2Pass	3	7.1362	3.83%	1.1674	78.47%

Table 2. General performance data of the denser 1.87 million points grid

Case	stator blades	mass flow [kg/s]	relative mass flow error	π_{stat}	η_{is}
Without_less	1	7.3567	0.00%	1.1702	84.95%
With_less_2pass	3	7.0861	3.68%	1.1669	76.58%
With_less_4Pass	5	7.2155	1.92%	1.1686	79.77%

Table 3. General performance data of the coarser 1.12 million points grid

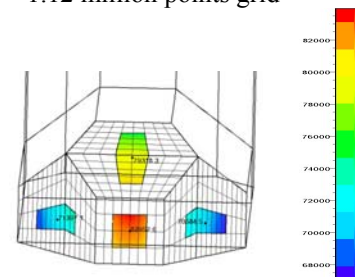


Fig.16. Static pressure at the measurement holes (With_rot_2pass)

Case	Local values [Pa]				Surface Average [Pa]			
	p_1	p_2	p_3	p_4	p_1	p_2	p_3	p_4
With_rot_2pass	82952.6	70584.5	71397.1	79318.3	82609.8	70465.9	71243	78895.7
With_less_2pass	79840.4	67871.9	68498.3	78623.4	79521.5	68377.6	67775.6	78168.6
With_less_4pass	80080.0	69014.1	68051.2	78561.0	79762.3	68893.9	67950.5	78110.8

Table 4. Pressures at the measuring points

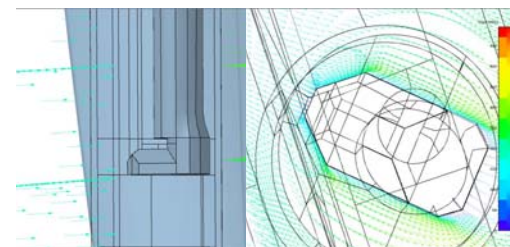


Fig.17. Flow velocity vectors at probe head

In order to obtain the primary flow components an iteration process is performed using the experimental calibration data of the probe "Sonde F" and an existing program of the Turbomachinery Laboratory of the Leibniz University of Hannover (Appendix A). Table 5 shows the resulting velocity magnitude and the

flow angles α and γ compared to the values of the computations without probe and the experiment.

When a comparison is made between the CFD results and the experimental values it is essential, at first, to distinguish between the CFD results of the case without the probe and the cases with the probe. As it has been said the CFD results have been performed with the boundary conditions set in such a value so as to correspond to the case when the 4AV compressor is working at its highest efficiency. However, as it is presented in Fig. 6, there is a significant difference between the mass flow of the highest efficiency point as computed with CFD and as measured at the experiment. The mass flow for the experiment is 7.87 kg/s while for the CFD is around 7.4 kg/s. Thus, since the CFD cases correspond to almost 6% lower mass flow, it is expected for the experimental values of the velocity to be slightly higher than the ones of the CFD computations. As it can be seen in Table 5, the results of the CFD cases without the probe and the experimental measurements present satisfactory agreement for both flow angles, having a deviation of one degree, while the velocity is taking approximately 5% lower values for the CFD results. Hence, it can be said that the CFD simulations for both grids without the probe are describing adequately the flow field of the compressor.

At the next step of the comparison, regarding the CFD cases with the probe, it can be said that the values of α are acceptable since they differ only marginally within a range which can be seen as a numerical error. However, the examination of the γ angle as well as of the velocity magnitude \bar{C} reveals obvious differences with the experiment and the cases without the probe, which might be even more appropriate since they correspond to a more comparable mass flow.

First, looking at \bar{C} , it can be stated that the gap between the computations with and without probe is significant, as a systematic error seems to underlie in the calculations of this quantity. The same can be said about the pitch angle γ . In contrast with the empty grids, all angles calculated during the calibration process for the CFD cases with the probe have a negative sign. This is an unreasonable solution as Fig. 17 shows that the flow streams from the hub to the shroud and always has a positive sign. To understand this systematic error, a look at the probe calibration data and the way they were obtained is necessary. As, already, mentioned the data resulted from experiments in a high-velocity calibration tunnel, so that they can be regarded as very precise to use in the experiments. These calibration coefficients are valid for the actual probe but do not correspond 100% with the CFD computations.

The reasons for this inconsistency can be looked in the grid of the probe and more specifically in the discretization of the regions of the pressure holes. As it can be seen in Fig.16 the pressure holes are modeled as solid parts of the probe, something which is not accurately compatible with reality. Thus, even the usage of a surface-average function cannot provide the same pressure value as it would be measured if the probe holes were modeled as they are in the real construction. In addition, several simplifications of the probe (Appendix B) were used during the meshing process which however small they might be they might increase the structural differences of the CFD probe model with the real geometry.

Because of these factors, the calibration data does not fit. A brief calculation (without any iteration procedure) of the PAC of the With_less_4pass (surface) case shows the origin of the systematic error:

$$PAC = \frac{p_1 - p_4}{p_1 - \frac{(p_2 + p_3)}{2}} = \frac{79762.3 - 78110.8}{79762.3 - \frac{(68893.9 + 67950.5)}{2}} = 0.15$$

For all Mach numbers the PAC graph (Appendix A) of the calibration data has a negative pitch angle γ for this value. Hence, the calibration data does not suit to the numerical model of the probe. Since the calculation of the TPC and SPC and, thus, p_{total} and p_{static} , rely on the correct determination of γ , the mistake affects also these quantities. Then, it can be assumed that the use of the experimental TPC and SPC graphs also leads to incorrect values.

Case	α [°]	γ [°]	C_{abs} [m/s]
experimental	-42.02	2.66	217.74
Without_full	-43.40	3.73	207.50
With_rot_2pass (local)	-43.54	-1.88	235.40
With_rot_2pass (surface)	-43.52	-1.64	235.40
Without_less	-43.50	3.89	208.76
With_less_2pass (local)	-43.43	-6.47	236.01
With_less_2pass (surface)	-42.58	-5.81	235.96
With_less_4pass (local)	-42.34	-5.53	235.70
With_less_4pass (surface)	-42.34	-5.24	235.70

Table 5. Primary flow components

Conclusions – Future actions

The present work dealt with the numerical investigation of the unsteady interactions between a pneumatic probe, the flow and the blades of an axial compressor. Especially the primary flow components velocity magnitude \bar{C} , yaw angle α and pitch angle γ were examined. Objects of this investigation were the first and a half stage (IGV, rotor 1 and stator 1) of the experimental 4AV compressor of the Turbomachinery Laboratory of the Leibniz University of Hannover and the four-hole cobra probe “Sonde F”. The creation and

analysis of compressor grids of varying density was presented. It revealed that in comparison with existing experimental data all computations showed a lower mass flow, efficiency and pressure ratio. A comparison of the meshes indicated that the errors decreased, when the density of the mesh was increased and that grid independence was reached at about 1.89 million points of the complete mesh. Furthermore, the investigations also showed a small error for a 1.12 million points grid. The points of highest efficiency (design point 2b) of both grids were determined and characteristic curves were plotted. Again, a difference to the experimental behavior was noticed, attributed to the insufficient numerical model of the compressor.

At the next step, a computational grid modeling the probe was created and inserted inside the initial grid of the compressor. Due to the usage of periodic boundary conditions the insertion of the probe grid into the compressor caused a high blockade of the duct. In order to weaken this blockade, Stator 1 was extended pitchwisely. The results showed a significant decrease of the blockade and the addition of two more stator blades on each side showed an even lower blockading effect (1.92% mass flow error).

Since the measuring holes were neglected during the meshing of the probe, the pressures were obtained as local values at the middle points of the former holes and as surface averages which approximated the holes. The experimental calibration data were used to calculate the primary flow components and the results were compared to the values of the compressor grids without the probe. The comparison showed, that the experimental calibration data did not fit to the numerical model for the cases of the pitch angle γ and the velocity magnitude \bar{C} . On the other hand the results of the yaw angle α were in accordance with the results of the grids without probe and with the experimental data indicating that the initial idea of the simulation with CFD methods of an experimental process can be workable.

Since the problem lie in the fact that the calibration data do not fit, it is important to correct them in order to correspond to the exact probe model used for the numerical simulations. In order to obtain fitting calibration data for the numerical model of the probe, a correction of the experimental data or a complete numerical calibration of the probe is necessary in the future. The numerical calibration can be done by installing the probe model grid in a grid simulating the flow field inside an empty windtunnel. Then, the probe calibration coefficients could be recalculated by following the exact same procedure as in the experiment but this time taking into account the pressures on the regions of the measurement holes as computed in the CFD results on the probe model

in the "windtunnel". As a next step, the results of Table 5 of the present work should be recalculated in order to be able to conclude about the effect of the interactions between the probe, the flow and the blades of the turbomachine, Fig.18.

In addition, the neglecting of the measuring holes of the probe requires further investigation regarding the advantages of obtaining the pressures as surface averages or as local values. This verification requires corrected calibration data. Future work could also re-add the holes to the probe grid as in the actual construction.

For future work, it is, also, recommended to develop further solutions of the thirty-probes problem in order to eliminate the blockade of the duct even more. A higher computer hardware capacity could allow the meshing of 180° of the Stator 1 stage, which would decrease the actual number of probes to two so that the CFD results with the probe could be accurately compared, at least, with the CFD case without the probe.

As it has been presented, this work was an effort of investigating the interaction between blades, probe and flow in a compressor. However, the unsteadiness of this interaction was disregarded as the computations were always done in the steady mode. This decision was based mainly on the current CPU and memory limitations since the unsteady computations would require a significantly higher computational capacity than the one applied in this work. Nevertheless, and taking into account the improvement of the available technology, unsteady simulations can be performed in the future especially if they can be combined in a numerical model of all 4AV stages which would allow the investigation of the influence of the probe-flow interaction on the whole compressor.

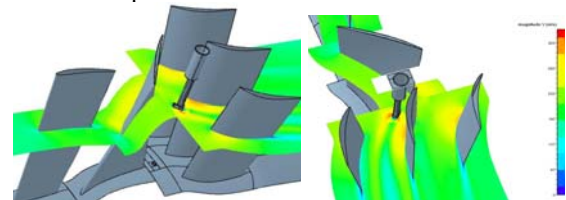


Fig.18. Velocity magnitude (With_less_2pass)

NOMENCLATURE

English letters

C	Velocity
c_p	Specific heat at constant pressure
C_x	Velocity component at x-direction
C_y	Velocity component at y-direction
C_z	Velocity component at z-direction
m	Mass flow
PAC	Pitch angle coefficient

p_i	Pressure at hole $i = 1,2,3,4$
p_{static}	Static pressure
$p_{stat,Pr}$	Static pressure measured by Prandtl tube
p_{total}	Total pressure
$p_{tot,Pr}$	Total pressure measured by Prandtl tube
SPC	Static pressure coefficient
TPC	Total pressure coefficient
T_{static}	Static temperature
T_{total}	Total temperature
YAC	Yaw angle coefficient

Greek letters

α	Yaw angle
γ	Pitch angle
η_{is}	Isentropic efficiency
κ	Isentropic coefficient
π_{stat}	Static pressure ratio

REFERENCES

1. Baldwin, B. S. and Lomax, H.: Thin Layer Approximation and Algebraic Model for Separated Turbulent Flows, AIAA Paper 78-257, 1978.
2. Braun, M. and Rieß, W.: Stationäres und instationäres Verhalten verschiedener Typen von Strömungsmesssonden in instationärer Strömung: (Strömungsmesssonden in instationärer Strömung). Abschlussbericht DFG-Normalverfahren, Ri 375/13-1, Institut für Strömungsmaschinen der Universität Hannover, Deutschland, 2003.
English title:
Braun, M. and Riess, W.: "Steady and unsteady behaviour of various types of probes in unsteady flow: (probes in unsteady flow). Final report DFG Individual Grants Program, RI 375/13-1, Laboratory of Turbomachinery, University of Hanover, Germany, 2003.
3. Braun, M. and Seume, J.: Experimentelle Untersuchung einer vorwärtsgepfeilten Beschaukelung in einem mehrstufigen Axialverdichter, FVV (Forschungsvereinigung Verbrennungskraftmaschinen e.V., Frankfurt), Abschlussbericht, Heft 800, 2005, Frankfurt, Deutschland, 2005.
English title:

Braun, M., Seume, J.: Experimental investigation of sweep blading in a multi-stage axial compressor, FVV, Final report, Issue 800, Frankfurt, Germany, 2005.

4. NUMECA International: FINE User Manual, Version 6.2, September 2004.
5. NUMECA International: How to? generate grids for turbulent flows, 1st Edition. Quick Reference Card No 2, June 15th 2001.
6. NUMECA International: IGG User Manual, Version 4.9-1, July 2004.
7. Seume, Jörg R.: Numerische Strömungsmechanik, Vorlesungsskript, Institut für Strömungsmaschinen der Universität Hannover, 2004.
English title:
Seume, J.: Numerical Fluid Mechanics, Lecture Notes, Laboratory of Turbomachinery, University of Hanover, Germany, 2004.
8. Spalart, P. R. and Allmaras, S. R.: A One-Equation Turbulence Model for Aerodynamic Flows, AIAA Paper 92-0439, 1992.

**Appendix A – Calibration Data and Iteration
Procedure**

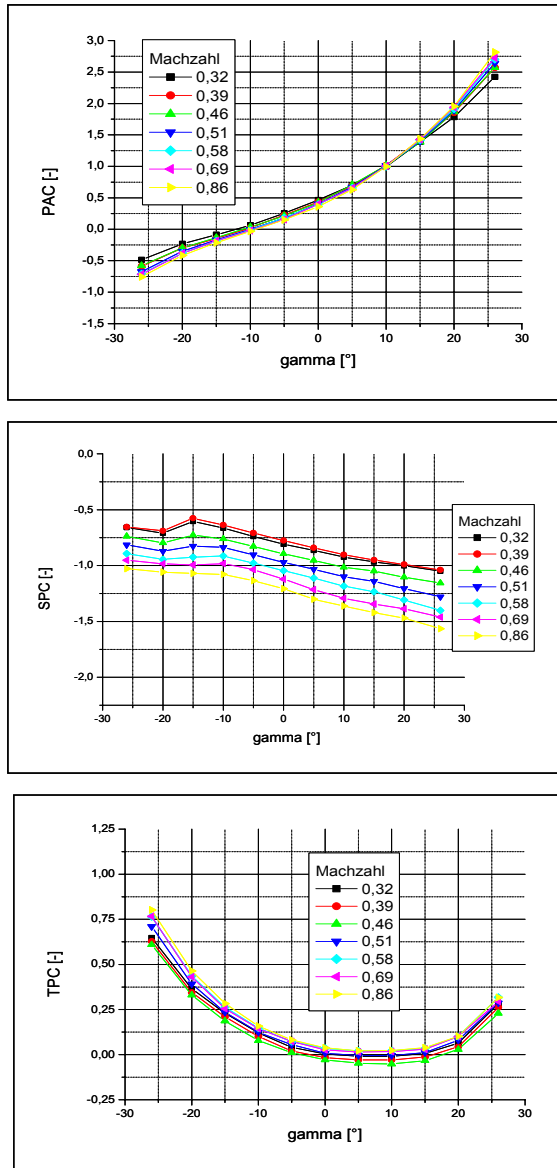


**Fig.A1. Probe “Sonde F” calibration data
(without YAC)**

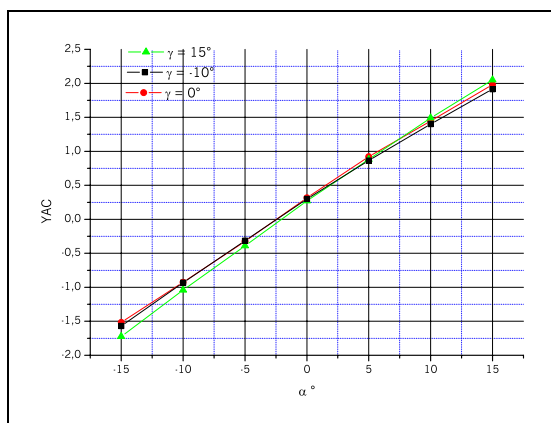


Fig. A2. Probe “Sonde F” calibration data YAC

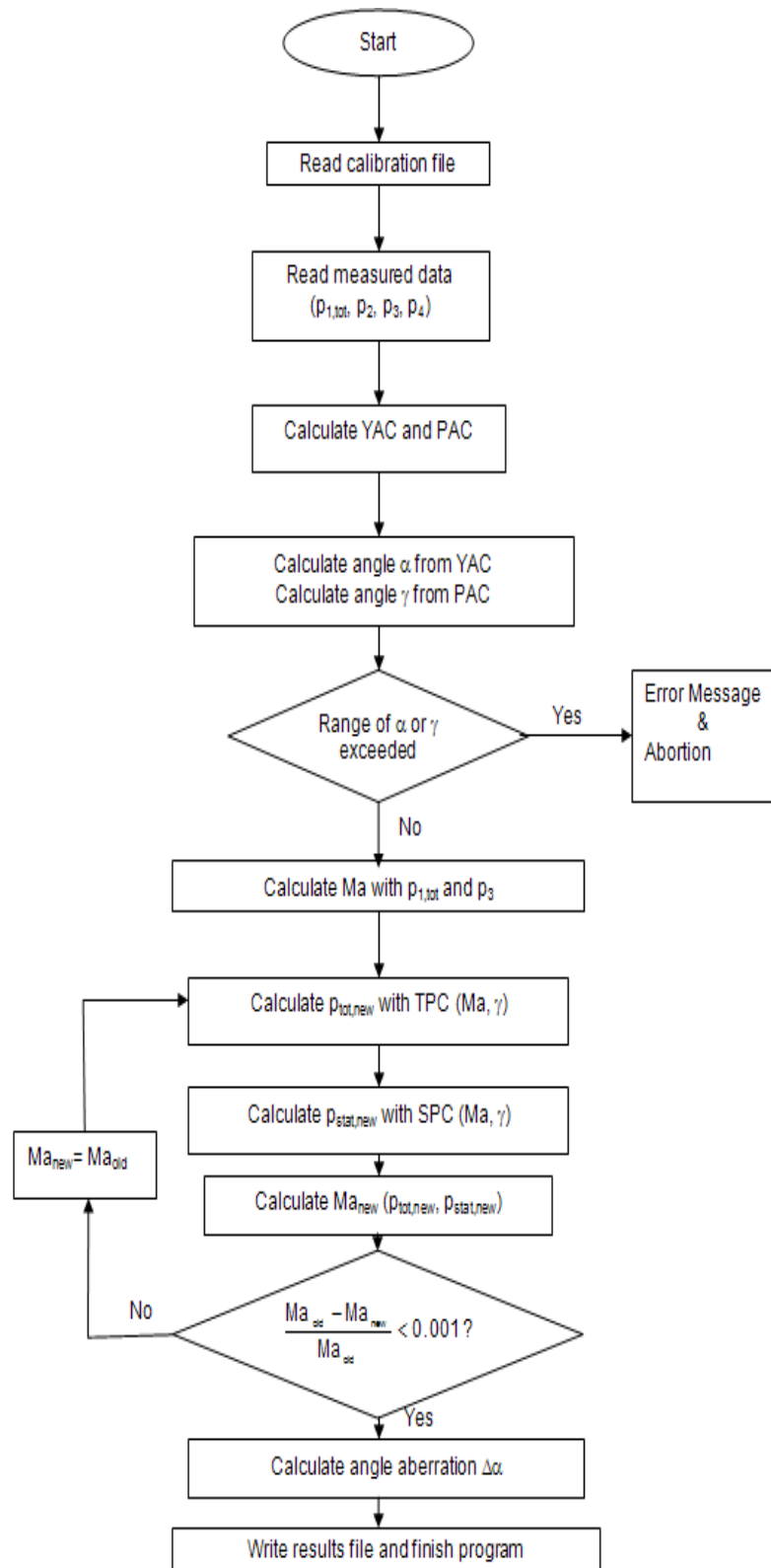


Fig.A3. Iteration procedure

Appendix B – Modeling of the probe

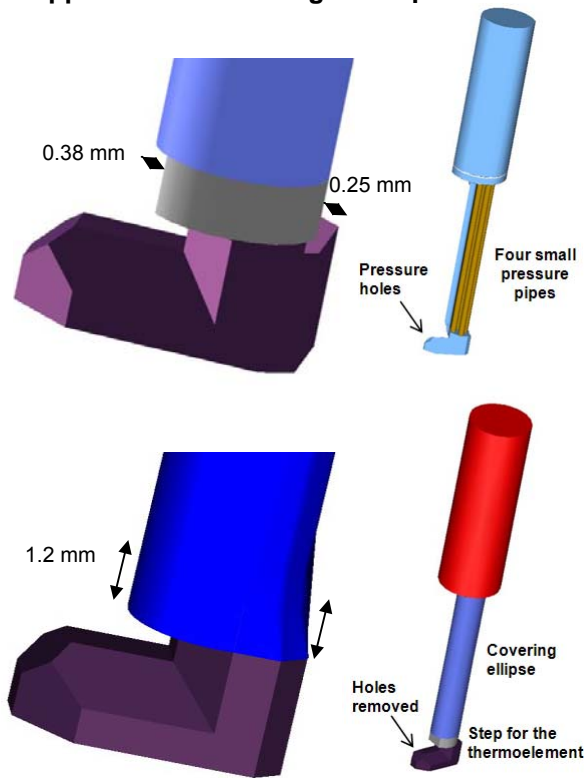


Fig.B1. Simplifications on the probe

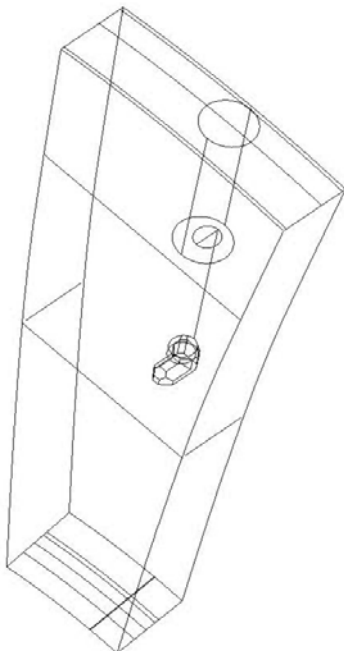


Fig.B2. Probe mesh boundaries

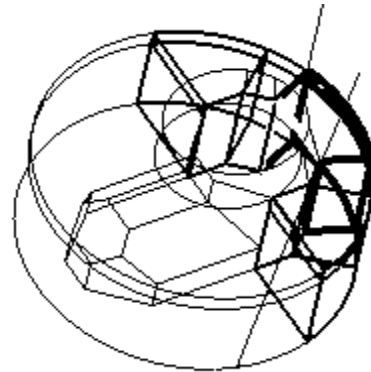


Fig.B3. Cylindrical boundaries and blocks at the probe head

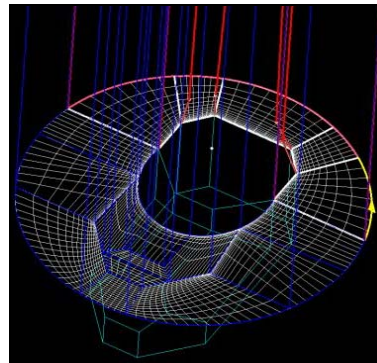


Fig.B4. Point distribution and clustering at two levels at the probe head